Biomass Conversion and Biorefinery
https://doi.org/10.1007/s13399-022-02987-z

ORIGINAL ARTICLE

Isolation and characterization of cellulose nanocrystals from *Ensete ventricosum* pseudo-stem fiber using acid hydrolysis

Abnet Mengesha Dube[1]

Received: 16 April 2022 / Revised: 8 June 2022 / Accepted: 21 June 2022

Abstract

Ensete ventricosum (false banana) is a common food source for a considerable section of Ethiopia's population in the central, southern, and southwestern areas. *Ensete ventricosum* pseudo-stem fiber is a type of agro-industrial waste that is widely available across the country. It has a limited number of known conventional applications and merits further investigations. One of the activities that prompted the completion of this study was the upgrading of *Ensete ventricosum* pseudo-stem fiber to value-added products such as cellulose nanocrystals. The goal of this study was to extract cellulose nanocrystals from *Ensete ventricosum* pseudo-stem fiber using sulfuric acid hydrolysis. An acid-catalyzed reaction technique using 1:20 mL cellulose to H_2SO_4 (51.1%) ratio and hydrolysis period of 52 min at 51 °C reaction conditions was used to separate cellulose nanocrystals from *Ensete ventricosum* pseudo-stem fiber cellulose. Thermal stability, crystallinity, surface charge, shape, size, and functional changes were all assessed in the cellulose nanocrystals that resulted. It had a better crystallinity index (78.0%), an average particle size of 66.7 nm, a yield of 39.78%, good thermal stability (> 300 °C), and a morphologically comparable rod-shaped structure. As a result, it is feasible to conclude that *Ensete ventricosum* pseudo-stem fiber offers a lot of potential for isolating cellulose nanocrystals for various applications.

Keywords Biowaste · *Ensete ventricosum* · Pseudo-stem fiber · Biomass conversion · Cellulose · Cellulose nanocrystals

1 Introduction

The period of petroleum and petroleum-based products to meet world economic requirements is shortened due to finite petroleum resources, increased costs, rapid population growth, and decisive environmental impacts [8]. Agro-waste and forest leftovers can be used as viable alternatives to petroleum and petroleum-based goods since they are natural, renewable, abundant, sustainable, and ecologically benign [34]. The world's attention has now switched entirely to the development of suitable materials, chemicals, and raw materials derived from sustainable and renewable sources [94]. Agro-wastes, which are the largest source, are underutilized and discharged into the environment as waste, and are the logical alternatives to petroleum and petroleum-based products [22]. These lignocellulosic biomass wastes are a valuable resource that can be found in abundance in all parts of the world, and they have the potential to support the long-term development of materials like nanocrystals and nanocomposite, as well as the production of liquid and gaseous bioenergy like biofuels, biodiesels, and bioethanol [65]. As a result, lignocellulosic biomasses are the most plentiful renewable feedstocks for cellulose manufacturing [19, 99].

Lignocellulosic biomass from various sources has emerged as the most promising and possible renewable raw resource for the production of cellulose. Because of their availability and low cost, several plant sources with varying quantities of cellulose have recently been employed for cellulose extraction [2]. Corn straw, banana leftovers, forest trash, wood chips, wheat straw, and flax fiber are the most common plant sources for cellulose extraction [6, 24, 35],Q. [104].

Because of their higher crystallinity index and huge volumes of cellulose, fibrous agricultural wastes are a preferred source of cellulose for the production of cellulose nanocrystals [6, 17, 19, 21]. One of these fibrous sources of raw materials for cellulose extraction is *Ensete ventricosum*

✉ Abnet Mengesha Dube
abnetm817@gmail.com; abnet.mengesha@wku.edu.et

[1] Department of Chemical Engineering, College of Engineering and Technology, Wolkite University, Gurage Zone, P.O. Box: 07, Wolkite, SNNPR, Ethiopia

Published online: 02 July 2022

pseudo-stem fiber (EVPSF). It could be used to isolate cellulose nanocrystals as a more preferred new cellulosic source.

Ensete ventricosum, often known as false banana, is a plant that belongs to the genus Ensete, which is part of the Musaceae Ensete family and the Scitamineae order (A [1, 16],Nurfeta, Eik, et al., 2008; [101]. Although *Ensete ventricosum* shows morphological similarities to banana plants, banana plants belong to the Musa genus, which is linked to *Ensete ventricosum*. The *Ensete ventricosum* plant is widely farmed in central, eastern, and sub-Saharan African countries, and it is one of Ethiopia's primary food crops, consumed by about 20% of the population in the country's southern, southwestern, and central regions [15, 67, 68, 95, 101]. The leaf lamina, leaf midribs, pseudo-stem, and corm are the four fractional portions that make up the dry matter of *Ensete ventricosum* (Nurfeta, Eik, et al., 2008). As a byproduct of the Kocho production process, a large amount of EVPSF was discharged in the environment [13, 101]. This fiber is a lignocellulosic biomass source for cellulose extraction [13, 94, 101]. EVPSF has cellulose content ranging from 58.75 to 64.9% wt., hemicellulose content ranging from 17.82 to 27.88% wt., and lignin content ranging from 6.33 to 11.35% wt. [14, 27, 94] with a crystallinity index of 64.9% [94]. EVPSFs are currently utilized to manufacture sacks, bags, ropes, cordage, mates, and sieves, as well as used as construction tying materials in lieu of nails [94]. High cellulose content, low hemicellulose, lignin, and extractives, and a high crystallinity index are just a few of the benefits of this fiber. It is also underutilized, renewable, inexpensive, agro-waste, readily available, and plentiful. As a result, it could be a viable cellulosic biomass for the production of cellulose nanocrystals (CNCs).

CNCs are created using various types of acid hydrolysis, such as hydrochloric acid, sulfuric acid, and various organic acids [64, 98]. Sulfuric acid hydrolysis is a common method for producing CNCs from biomass resources. Sulfuric acid is the most preferred and widely used acid for acid hydrolysis extraction of CNCs due to its strong isolation properties, ability to form a stable colloidal system, and esterification of hydroxyl groups by sulfate ions [23, 50]. The acid is hydrolyzed with less organized regions such as amorphous and aromatic polymers in this method, but the alpha cellulose is tightly bound, limiting access to the crystalline region and leading to acid resistance (Nagarajan, Balaji, Thanga Kasi Rajan, et al., 2019).

CNCs with nanometer-sized dimensions are natural-based materials with unique and potential properties [32],TAPPI International Nanotecnology Division & [90]. These crystalline materials have a rod-like structure, nanoscale width and length, and a high crystallinity index [46]. When compared to their natural cellulosic fiber counterparts, cellulose nanocrystals exhibit superior mechanical strength, stiffness, biodegradability, and specific surface area. They also offer superior qualities when compared to other materials such as steel wires, Kevlar, synthetic polymers, cellulose nanofibril, and cellulose nano-whiskers, which are employed in a variety of applications [10, 47, 58]. Many researchers reported cellulose nanocrystal applications in food packaging, medical tools, drug delivery, nanocomposite in polymers, biosensors, cosmetics, and pharmaceuticals, as well as applications in other areas of nanotechnology [32, 47],Nagarajan, Balaji, Ramanujam, et al., 2019).

The purpose of this study was to extract cellulose nanocrystals from EVPSF cellulose using sulfuric acid hydrolysis. Excellent-quality cellulose was extracted under good and optimal process conditions by carefully removing wax, lignin, hemicellulose, and other trace components. The extracted cellulose was used to create cellulose nanocrystals in an acidic media by treating it with sulfuric acid. The cellulose nanocrystals, cellulose, and raw fibers that resulted were all characterized.

2 Materials and methods

2.1 Materials

EVPSF that had been freshly extracted and used as a raw material for this study was obtained from local farms (Endiber town, Gurage zone, South Nation, Nationality and People Region, Ethiopia). Thimbles for Soxhlet extraction, cellulose membrane (D9402, Sigma-Aldrich), sodium hydroxide (97%), sulfuric acid (97%), ethanol (97%), toluene (99%), sodium chlorite, sodium bisulphite, acetic acid (99.5%), hydrogen peroxide, and chloroform (99%) were all purchased on the global chemical market (Sigma-Aldrich, Fine Chemicals PLC, Addis Ababa, Ethiopia). All of the chemicals and reagents utilized in this study were analytical grade, which meant they did not need to be purified further.

2.2 Extraction of CNCs from *EVPSF*

2.2.1 Mechanical treatment

Fresh *EVPSF* was chopped into 4–10 mm and soaked in distilled water for about 24 h to remove water–soluble solid dirt and impurities. The cleaned fiber was then air dried for 5 days before being oven dried for 2 days at 80 °C. To obtain powder fiber, dried fiber is pulverized in a high-speed multi-purpose crusher (1000A, China) and sieved through 40–60 mesh sieves [77]. Soxhlet extraction (Buchi E-816, Switzerland) was employed using an ethanol-toluene (1:2 v/v) solvent with a fiber to solvent ratio of 1:10 w/v for two successive extraction cycles of 6 h each at 78 °C to remove extractive components of the fiber (wax, pectin, oil, etc.). Following a series of preliminary studies, the extraction

conditions such as solvent type and ratios, fiber to solvent ratio, and extraction temperature were identified. Finally, the dewaxed fiber was rinsed several times with distilled water to remove solvents, and then dried overnight in a 45 °C.

2.2.2 Alkali treatment

The alkali treatment was utilized to purify the cellulose by eliminating a substantial percentage of hemicellulose and partially removing lignin from EVPSF [32]. The ground and wax-free EVPSF was treated three times with an alkali solution of sodium hydroxide (4%) at a solid to liquid ratio of 1:20 (w/v) with continuous agitation at 750 rpm for 3 h at 75 °C. To remove sodium hydroxide that had adhered to the surface of the solid cake, it was filtered and washed many times with distilled water until a neutral pH was achieved. The concentration of OH^- ions reduces when an alkali is diluted with water. As more water is added, the pH of the alkali falls towards 7, making the solution less alkaline [71]. After filtering and washing, the solid residue was dried overnight at 45 °C.

2.2.3 Oxidation treatment (bleaching)

Prior to bleaching, alkali-treated EVPSF was ground and then bleached twice under mechanical string at 55 °C for 2:30 h using equal parts (v/v) of a 24% wt. H_2O_2 solution and an aqueous solution of sodium hydroxide (NaOH) and glacial acetic acid (2.7% wt./v NaOH and 7.5 v/v% acetic acid) with a fiber to solution ratio of 1 g the bleached fiber was then cooled in the reactor, filtered, and washed many times with distilled water until it reached a neutral pH, and then dried in an air-circulated oven at 40 °C for 24 h. Following a preliminary experiment and a review of the literature, all of the bleaching conditions were identified [100, 102].

2.2.4 Acid hydrolysis

An acid-catalyzed reaction technique was used to separate CNCs from EVPSF cellulose. The hydrolysis took 52 min at 51 °C and used 51% sulfuric acid. A tenfold amount of cold distilled water was used to stop the hydrolysis process [48]. Hydrolyzed CNCs were washed and centrifuged at 4000 rpm for 20 min to separate excess sulfuric acid three times. To eliminate non-reactive salts and soluble sugars from the extracted CNCs, dialysis against distilled water was done repeatedly for 5 days [81]. Every day, the distilled water used in this process was changed. To achieve a uniform suspension, the CNC suspension was ultrasonicated for 10 min. The suspension of the CNC was then kept at 4 °C. This method was derived from past works and from trial and error experiments (Johar et al., 2012a,[41, 49, 59, 83, 87].

2.3 Characterization of *EVPSF* and cellulose nanocrystals

2.3.1 Chemical composition of raw and treated EVPSF

The quantities of ash, moisture, extractives, acid-insoluble lignin, cellulose (β, γ, and α), holocellulose, and hemicellulose in EVPSF were determined using various standards. Aldaeus and Sjoholm (2011) procedures were used to determine the moisture content of the fiber. Five grams of EVPSF were dried in an air-circulated oven (FD-56) at 105 °C until a consistent weight was achieved [4]. The result was calculated using Eq. (1). The ash content of the fiber was determined in accordance with the Technical Association of the Pulp and Paper Industry (TAPPI) standard and Silverio (2013) protocols [84, 89]. The *Ensete ventricosum* fiber sample was combusted using a muffle furnace (MF-106) at 525 ± 25 °C and the result was calculated as Eq. (2).

$$\%Moisturecontent = \left(\frac{Initialsampleweight - Driedsanpleweight}{Initialsampleweight}\right) * 100 \quad (1)$$

$$\%Ash = \left(\frac{Weightofash}{Weightofash}\right) \times 100 \quad (2)$$

Extractives, acid-insoluble lignin, α, β, and γ cellulose, and holocellulose content were determined according to different TAPPI standards. T 204 cm-97 [18, 88],Tappi T 204 cm-97, 1997) for extractives, T 222 om-02 [4, 92] for acid-insoluble lignin, T 203 (TAPPI 1999) for α, β, and γ cellulose, and American Society for Testing and Materials standard (ASTMS) D1104-56 for holocellulose contents, respectively.

2.3.2 Cellulose nanocrystals yield determination

CNCs suspension was freeze-dried to obtain powder CNCs and the yield of the process was calculated using Eq. (3).

$$\%YieldofCNCs = \left(\frac{WeightoffreezedriedCNCs}{weightofbleachedcellulose}\right)*_{100} \quad (3)$$

2.3.3 Particle size analysis

The particle size distribution and average particle size of the obtained cellulose nanocrystals were determined by using dynamic light scattering technology [31]. About 0.5 g of freeze-dried obtained cellulose nanocrystals were dispersed in 100 mL of distilled water and sonicated for 10 min using an ultrasonicator (Soniprep 150 plus) at 16 kHz. Prior to analysis, 0.05 mL of sonicated suspension was further diluted in 50 mL of distilled water. Then,

measurement was conducted using a Zetasizer Nano particle analyzer (ZE-3600) with a calibration time of 60 s at room temperature with a noise ratio of 1.02 for each sample three times, and the mean data was recorded.

2.3.4 Zeta potential analysis

The zeta potential of suspension of cellulose nanocrystals was measured by a Zetasizer Nano particle analyzer (ZE-3600) to determine the magnitude of the electrostatic force. The diluted suspension sample prepared under particle size analysis was used to record the zeta potential of cellulose nanocrystals obtained in this study.

2.3.5 Fourier transform infrared spectroscopy (FTIR)

Thermo Scientific (iS50 ABX) FTIR spectrophotometer was used to obtain spectra for raw *EVPSF*, extracted cellulose, and cellulose nanocrystals. The samples were ground and mixed with KBr to prepare pastilles [72]. The experiments were executed using infrared range of 4000–400 cm^{-1} with optical velocity of 0.15, resolution of 16 cm^{-1}, and a total of 32 scans for each sample.

2.3.6 Thermogravimetric analysis (TGA)

Thermal analysis of the raw, treated fiber of *EVPSF*, and isolated cellulose nanocrystals was performed to determine the thermal stability of the samples on a high precision TGA analyzer (HTC_1). About 5 mg of all dried and ground samples were heated at a heating rate of 20 °C/min from room temperature to 700 °C under a nitrogen atmosphere in a platinum crucible for about 1 h.

2.3.7 X-ray diffraction (XRD)

The degree of change in crystallinity index of all samples of raw and treated EVPSF and extracted cellulose nanocrystals was calculated from the integrated area of XRD data. For this analysis, an X-ray diffractometer (XRD-7000 X-ray Diffractometer, Shimadzu Corporation, Japan) was used to obtain X-ray diffraction patterns of different powder samples that were scanned at room temperature between 2θ with a diffraction angle in the range of 10° to 80° and a step size of 0.02°. Then, the sample crystallinity index ($\%C_I$) was determined by Eq. (4) [82, 97]:

$$CI = \frac{\left(\frac{1200-Iam}{1200}\right)}{\%CI = \left(\frac{1200-Iam}{1200}\right)*_{100}} \quad (4)$$

where I_{200} is the maximum peak intensity of diffraction at peak (2θ = 22.65°) corresponding to both the crystalline and amorphous regions, and I_{am} is the peak intensity of the amorphous region only at peak (2θ = 18).

2.3.8 Scanning electron microscopy (SEM)

A scanning electron microscope was used to evaluate the surface morphology of raw and treated fiber and cellulose nanocrystals from an *Ensete ventricosum* pseudo-stem by scanning the surface with a focused beam of electrons using SEM (JCM-6000Plus). Before analysis, the samples were gold coated (40–50 nm) and observed at a 500–10 µm working distance with an accelerating voltage of 15 kV under high vacuum.

3 Results and discussion

3.1 Chemical composition of *EVPSF* and determination of cellulose nanocrystal yield

Table 1 summarizes the results of determining the chemical compositions of EVPSF at the initial and final stages of each chemical pretreatment. Results for raw *EVPSF* showed higher holocellulose, 77.74% wt., and lower lignin, 6.68% wt., contents. These findings show that the fiber has a high potential for producing cellulose nanocrystals [42, 54, 86, 96]. After pretreatment, the holocellulose of the fiber was increased to 86.67% wt., while hemicellulose and lignin were decreased to 2.16 and 1.01% wt., respectively. At the end of the bleaching process, 83.03% wt. alpha cellulose was obtained. The chemical composition for the present work is in good agreement with other researchers' findings. Kargarzadeh et al. [42], who extracted CNCs from kenaf bast fibers, reported cellulose content after bleaching treatment as

Table 1 Chemical composition of EVPSF and isolated cellulose

Sample	Chemical composition%								
	Moisture	Ash	Extractives	Acid-insoluble lignin	α-cellulose	β-cellulose	γ-cellulose	Holocellulose	Hemicellulose
EVPSF	7.72	4.3	3.567	6.677	54.3515	1.87266	1.25018	77.736	20.26166
Treated EVPSF	7.639	3.94	0.7134	3.57	76.108	1.66278	1.10852	84.13766	5.25836
Bleached EVPSF	7.639	3.97	0.7134	1.010333	83.026	0.88791	0.59194	86.66727	2.16142

91.0% wt. [42]. Another researcher, Mariano et al. [54], also reported alpha cellulose as 72.43% wt. to isolate CNCs from sisal fiber [54]. The result of this study indicates that *EVPSF* is one of the cellulose sources to extract CNCs (Fig. 1).

3.2 Cellulose nanocrystals yield

At approximate optimum parameters' conditions (51% wt., 52 °C, and 51 min), CNCs extraction was performed three times. The mean yield of CNCs was recorded at 39.82% wt. This work's yield is consistent with the yields of Mengkuang leaves (28%), Saharan aloe vera cactus fibers (32%), sisal (30%), and rejected fibers (36.6%) reported by Ilyas et al., K. J. et al., Gracia de Rodriguez et al., and Aguayo et al., respectively [3, 29, 36, 40].

3.3 Particle size and zeta potential analysis

As Fig. 2A illustrates, the particles are distributed under two different peaks. The first peak covers almost 75.40% of the intensity of the particle distribution, and the second peak covers the remaining 24.60%. Table 2 also summarizes the particle size for these two peaks as 66.8 and 0.68 nm, respectively. As an alternative, it can be possible to report particle size distribution by percent of volume. Accordingly, Fig. 2B shows the particle distribution under two different peaks. Peak 1 covers 89.45% of the volume, and peak 2 covers the remaining 10.55% of the particle distribution by volume. The result for size in the case of volume distribution was recorded as 85.5 and 1.53 nm for peak 1 and peak 2, respectively. In both cases, there is an extremely low size of particles due to the vigorous acid hydrolysis conditions

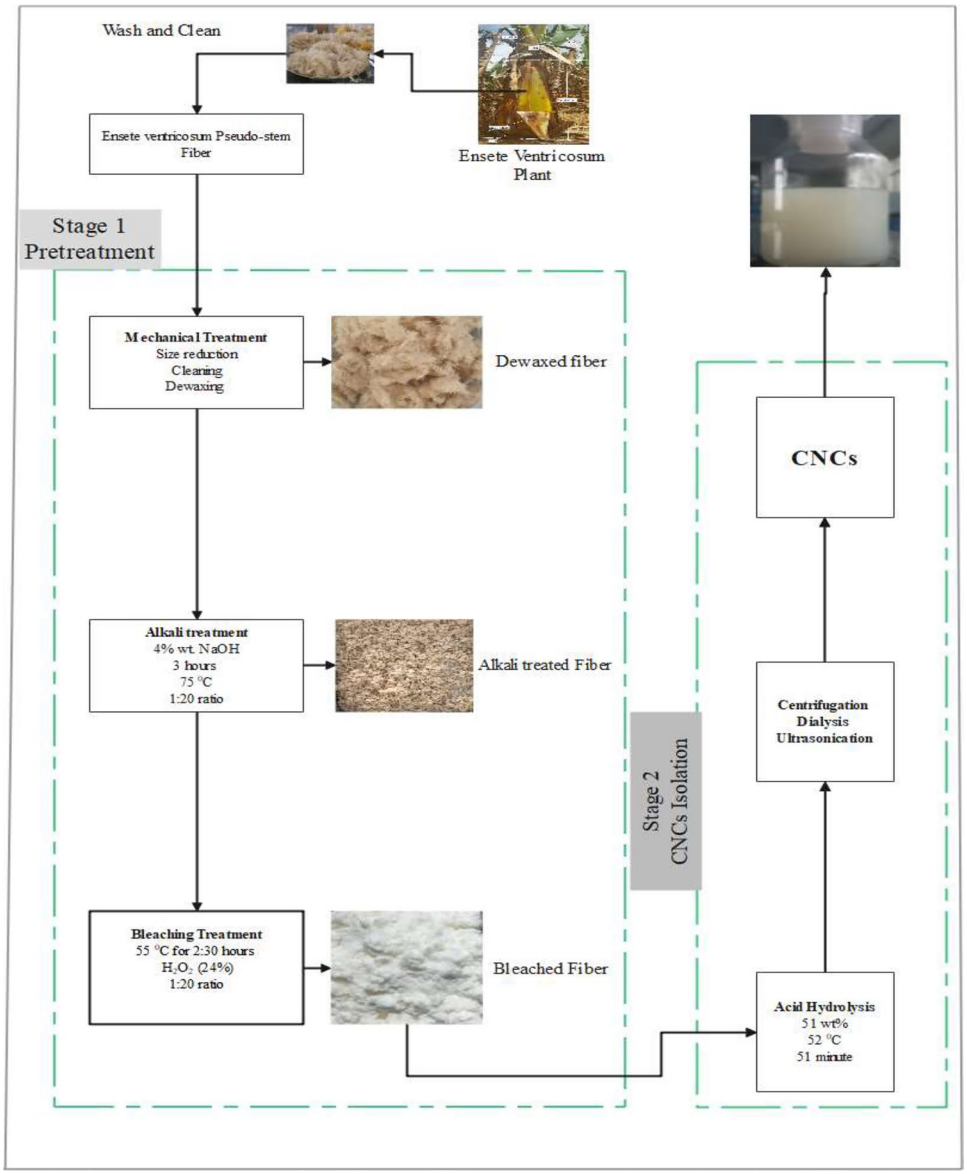

Fig. 1 Schematic illustration for the raw material preparation, pretreatments, and process of isolating CNCs from EVPSF

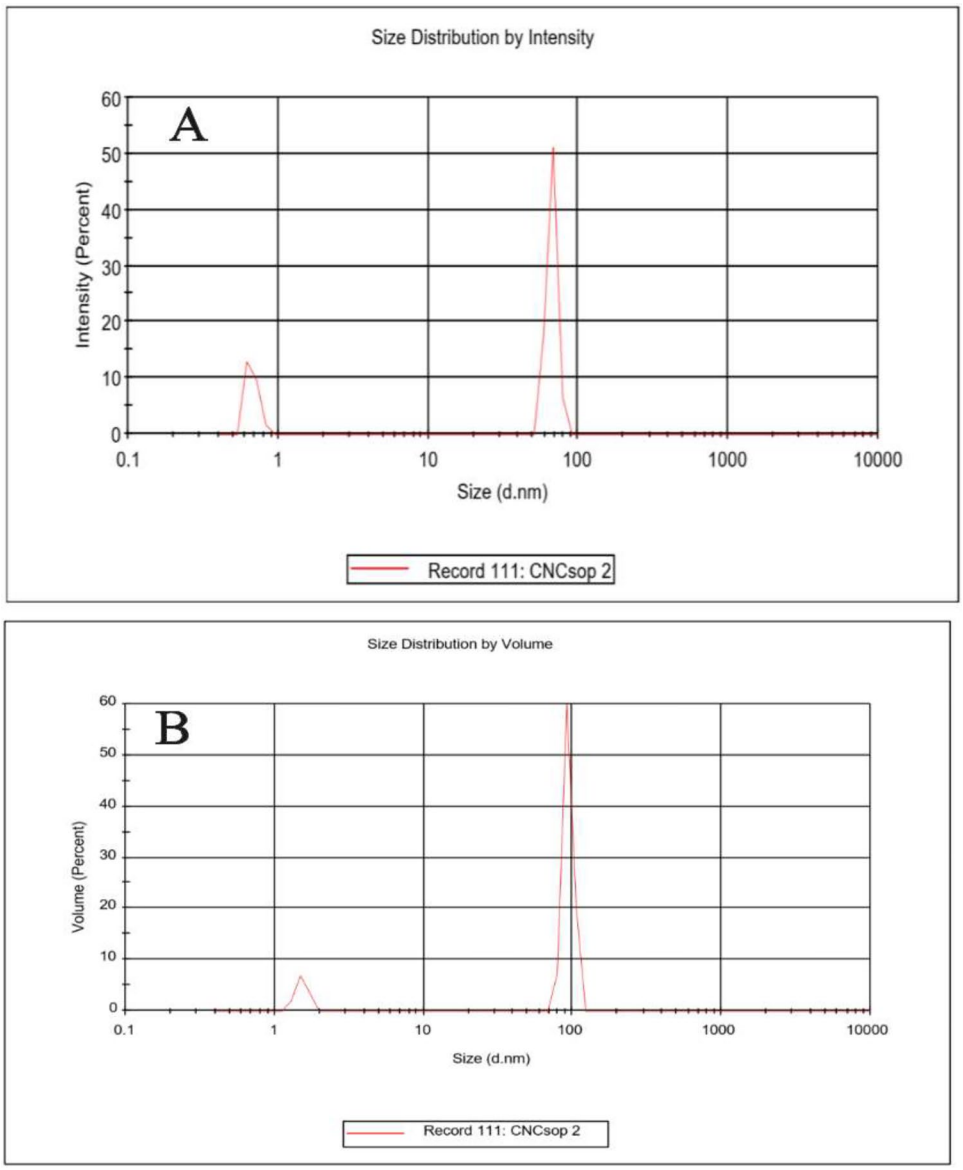

Fig. 2 Particle size distribution for CNCs by intensity (**A**) and volume (**B**)

Table 2 Particle size and their percent distribution in terms of intensity and volume

	Size distribution by intensity			**Size distribution by volume**		
	Size (d. nm)	% intensity/ volume	St dev (d. nm)	Size (d. nm)	% intensity/ volume	St dev (d. nm)
Peak 1	66.80	75.4	5.366	85.50	89.45	4.484
Peak 2	0.6758	24.6	0.064	1.532	10.55	0.06417
Peak 3	0.00	0.0	0.0	0.00	0.0	0.0
***z*-average (d. nm)**		**PDI**	**Intercept**	**Result quality**		
5151		0.17	0.774	Good		

of the crystalline region [74]. The average particle size of the CNCs is highly dependent on acid hydrolysis parameters [74]. Acid concentration can greatly affect the hydrogen bonds between cellulose polymers and can decrease the size of the CNC particles. The role of ultrasonication is also very significant in obtaining cellulose nanocrystal dispersion with a uniform (narrow) size distribution [38, 85]. Table 2 also contains results for hydrodynamic diameter (ZD),

polydispersity index (PDI), and the quality of the results. The average size result obtained in this study is a good result and indicates the isolation of CNCs from *EVPSF's* cellulose is a promising alternative. Depending on the source of cellulose, pretreatment methods, and isolation techniques, nanoparticles widely vary in their size [12, 29, 38, 70, 75]. Zhang et al. [103] reported the average particle size of CNCs isolated from lemon seeds as 100–350 nm,Asrofi et al. [9] reported the size of CNCs from water hyacinth fiber as 25 nm,Mandal and Chakrabarty [51] extracted CNCs from helicteres isora plant and reported the particle size as (10–100) nm,and Feng Jiang and You-LO Hsieh (2012) reported the diameter of cellulose nanocrystals from rice straw extracted by acid hydrolysis as 3.96–6.74 nm. The findings for particle size in this study agreed with those reported previously[9, 20, 51],H. [103].

CNCs extracted from *EVPSF's* cellulose using sulfuric acid hydrolysis at a given condition were shown to have a − 39.47 mV zeta potential (ζ). The negative charge of the product was an expected result due to the presence of sulfate groups, which are created by the sulfuric acid hydrolysis process and have the potential to create anion on the surface of CNCs [42, 85]. This zeta potential result is in the range of desired results since it has the potential to stabilize CNCs suspension in water solution [38, 42, 80, 85]. The negative charge on the surface of particles ensures stable dispersibility (avoiding agglomeration problems by electrostatic repulsion force) of CNC suspensions in water [7, 83]. Smyth et al. [85] reported zeta potential for CNCs extracted from corn (Zea mays) agricultural residue using two different sulfuric acid conditions as − 28.3 ± 1.1 and − 43.0 ± 0.6 mV,Prasanna and Mitra [74] also reported zeta potential for CNCs, which were extracted from *Cucumis sativus* peels, as < − 30 mv; and Feng Jiang and You-LO Hsieh (2012) also reported zeta potential for rice straw as − 67 to − 57 mV. Thus, my finding is in good agreement with these results and suggests that *EVPSF* CNCs extracted at optimized sulfuric acid hydrolysis conditions are stable enough to be dispersed in water for different applications.

3.4 Functional group analysis

The effectiveness of chemical pretreatment in the extraction of CNCs from EVPSF's cellulose using acid hydrolysis was confirmed by FTIR spectra. Figure 3 reveals the recorded spectra and characteristic bands for raw, alkali-treated, bleached *Ensete* fiber, and isolated CNCs. Generally, 3277.00–3348, 2922.65–2924, 1740, 1600–1634.74, 1414.16, 1315.45–1327.48, 1018.75–1028.75, and 899 cm^{-1} were obtained as characteristic bands of FTIR spectra for raw, alkali-treated, and bleached *EVPSF*, and the isolated CNCs. The presence of a stretching vibration of the

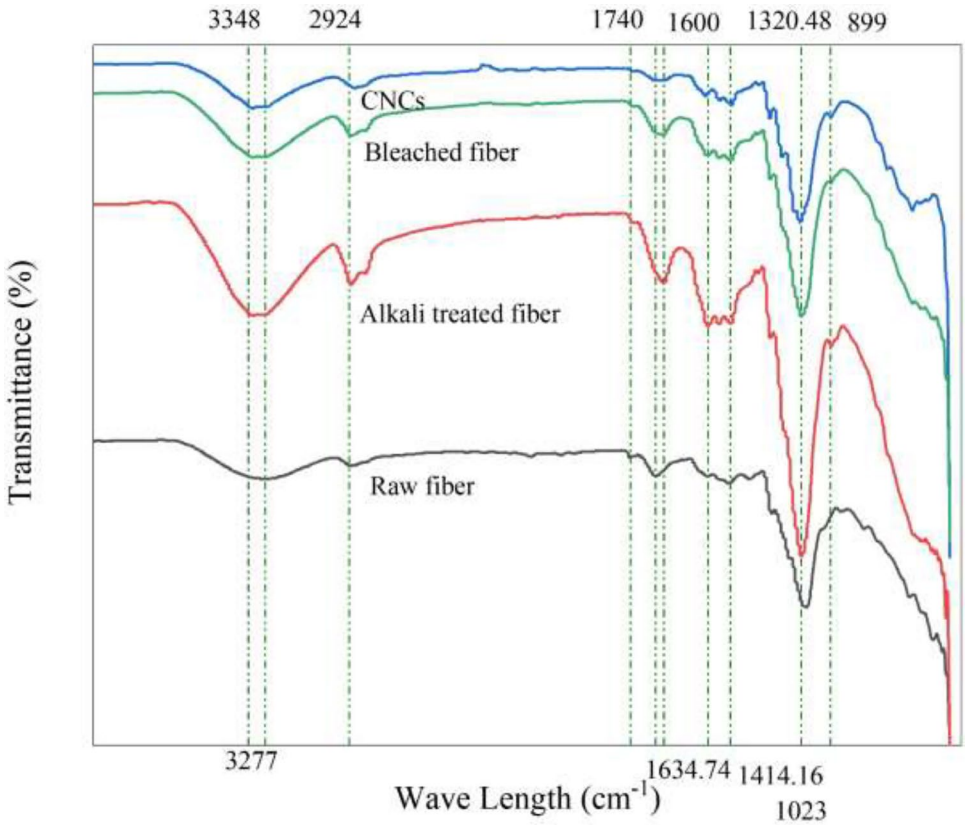

Fig. 3 FTIR spectra for raw, alkali-treated and bleached fiber, and extracted CNCs

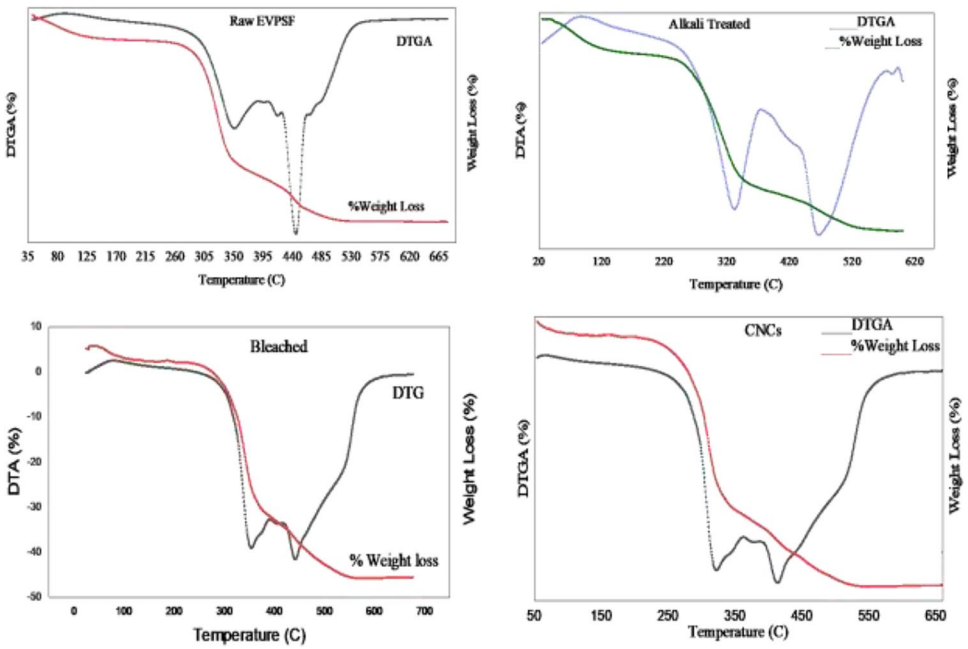

Fig. 4 TGA and DTGA curves of raw, alkali-treated, bleached EVPSF, and extracted CNCs

O–H group, which is related to the intramolecular hydrogen bond of cellulose, resulted in the characteristic band 3277.00–3348 cm^{-1} [41, 57]. As Fig. 3 clearly illustrates, the transmittance for this region gradually changes as chemical treatment of the fiber proceeds. Initially, the transmittance showed an increment due to alkali treatment and increase in cellulose content. At the end of chemical pretreatment, the transmittance decreased and the peak became sharper due to the removal of amorphous parts of cellulose. Totally speaking, in this broad band region, cellulose and CNCs show similar peaks except for a slight difference in peak intensity. The peak at 2922.65–2924 was assigned to C-H and CH_2 stretching vibrations for the aliphatic (methyl and methylene) group [41, 94]. This characteristic band indicates the presence of cellulose in *Ensete ventricosum* lignocellulosic biomass. After each chemical treatment, these peaks become sharp, and this situation indicates an increase in cellulose content [45]. The presence of a significant peak at about 1740 cm^{-1} is due to the C = O stretching of acetic and uronic ester groups of hemicellulose or ester linkage of the carboxylic groups of ferulic and p-coumaric acids of lignin [5, 79, 80]. This peak was gradually removed as it moved from raw to bleached fiber of the *Ensete ventricosum* pseudo-stem and finally disappeared completely from the final product, CNCs. Chemo pretreatments caused the disappearance of hemicellulose and lignin [5, 79]. 1634.74 cm^{-1} represents OH bending of adsorbed water (Hemmati et al., 2018a), whereas 1414.16 and 1327.74 cm^{-1} represent CH_2 scissoring of cellulose, hemicellulose, and lignin, and stretching of the C-O ring of syringyl of lignin and condensed G ring of lignin in *EVPSF*, respectively [95],H. [103]. Peak at 1315.45 cm^{-1} is associated with rocking vibration of CH_2 in alcohol group of cellulose [73], whereas peak at 1002 cm^{-1} illustrates the C–O–C pyranose vibrating stretching ring of cellulose [76]. Peak at 899 cm^{-1} depicts the normal cellulose structure with β-glycosidic bonds between glucose units in cellulose structure (Hemmati et al., 2018a,[94]. FTIR spectral result for the present work is in a good agreement with many research findings partially or fully [6, 37],Johar et al., 2012b,[52, 56, 72].

3.5 Thermal stability analysis

A thermal stability analysis was performed for raw, alkali-treated, bleached fiber of the *Ensete ventricosum* pseudo-stem and isolated cellulose nanocrystals using a TGA analyzer (Fig. 4). Figure 4 and Table 3 illustrate the TGA and DTG curves for all samples with their patterns of weight loss and thermal deterioration that occur at the maximum temperature of the samples. As the figure revealed, the weight loss during the thermal deterioration of samples occurs at three different temperatures. In the temperature range of room temperature to 150 °C, all samples showed an initial small mass loss (< 10%), which was directly related to free moisture evaporation and removal of low molecular weight components (Hemmati et al., 2018a; [55]. Cellulosic components were degraded in the second stage (185–400) °C of thermal degradation by depolymerization, dehydration, and glycosidic unit decomposition in almost all samples [43, 60, 66]. At this stage, TGA and DTG curves clearly showed that there was a difference between thermal degradation and weight loss patterns for raw, alkali-treated, and bleached *Ensete* fiber and isolated CNCs. The onset temperature (185.63 °C) of thermal deterioration of CNCs is

Table 3 Thermal analysis data for raw (R), alkali-treated, bleached (B) EVPSF, and CNCs

Sample	Evaporation of water			Degradation of cellulose chain			Degradation of carbonic residues			Residue% at end (> 600 °C) (°C)	DTGA peaks
	T_{onset} (°C)	T_{max} (°C)	WL (%)	T_{onset} (°C)	T_{max} (°C)	WL (%)	T_{onset} (°C)	T_{max} (°C)	WL (%)		
REVPSF	39	88	9.876	192.5	327.5	54.6713	417.5	485	17.382	13.883	350, 445.1673
ATEVPSF	28	54	5	238	338.5	58.712	413	483	17.6845	7.3273	332.16, 463.88
BEVPSF	39	55	5.011	247.5	352.5	65.462	396.25	466.25	14.7543	2.1852	355.06, 442.16
CNCs	45	76.25	5.201	185.625	325.625	62.47	365	500.63	13.86	3.835	322.82, 413.663

lower than bleached cellulose (247.5 °C), alkali-treated fiber (238 °C), and raw EVPSF (192.5 °C). According to Normand et al. [66], the thermal degradation of hemicellulose is in the range of 250–37 °C, for cellulose, it is estimated at 370–45 °C, and the whole range of thermal degradation is well fitted for lignin [66]. Therefore, the removal of non-cellulosic components, lignin, and hemicellulose resulted in a higher onset temperature for cellulose and alkali-treated fiber in the study. DTG curves reveal that the deterioration temperature of CNCs is declining faster and the T_{max} of cellulose nanocrystals is 325.63 °C, which is lower in comparison with bleached cellulose, 352.50 °C, alkali-treated fiber, 338.50 °C, and raw fiber, 327.50 °C. The nano-sized and negatively charged sulfate groups of CNCs are responsible for this faster thermal degradation [40, 55]. This may also be due to the replacement of hydroxyl groups during the hydrolysis step by sulfate groups, which makes CNCs less resistant to thermal degradation because of their lower activation energy [41]. Thus, sulfuric acid hydrolysis of *Ensete* fiber's cellulose into CNCs led to a great decline in thermal stability. Thermal deterioration of cellulose nanocrystals around 300 °C was found to be significantly related to the presence of negatively charged sulfate groups, which aid in the cellulose deterioration process [66, 69]. Several previous studies have shown that treating CNCs with sulfuric acid reduces their thermal stability significantly. Kallel et al. [41] showed that the thermal degradation of CNCs from garlic straw residues started at approximately 200 °C and ended at 370 °C [41]. Normand et al. [66] also reported that thermal deterioration of CNCs from spruce bark started around 190 °C and ended at 277 °C [66]. Oun and Rhim also reported the thermal degradation range for rice straw, wheat straw, and barley straw as 271–350, 265–370, and 265–35, respectively [69]. Other researchers, Hemmati et al. (2018b), recorded 230 °C as the thermal degradation starting point for CNCs from walnut shell agricultural residues (Hemmati et al., 2018b). Weight loss in this region is greatly related to the thermal degradation temperature range and sensitive parts of the sample to thermal degradation. Exposure to pyrolysis makes them lose a huge amount of weight. Raw *Ensete* fiber (54.7%), alkali-treated (58.7%), bleached samples (65.5%), and CNCs (62.5%) lost weight. These scenarios can be proven by other researchers' work (Hemmati et al., 2018a,[43, 66].

The third stage of thermal degradation due to oxidation and breakdown of charred residue takes place above 400 °C to form gaseous products of low molecular mass [93]. Due to the presence of ash and lignin, the charred percent of residue in raw *Ensete* fiber was higher than in alkali-treated and bleached cellulose. From the table, it was clearly observed that the char formation for CNCs was higher than bleached EVPSF. The free ends and high crystalline nature of CNCs that had large amounts of carbon were responsible for this

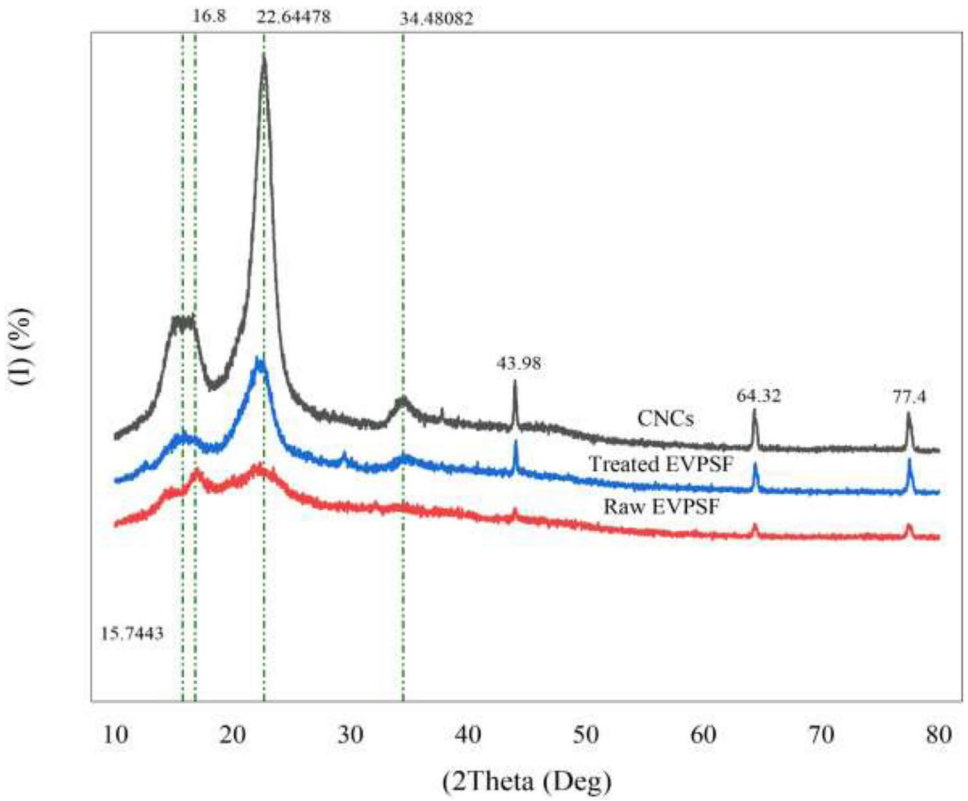

Fig. 5 XRD patterns of the raw, treated EVPSF, and isolated CNCs

situation [30]. Many different scholars have also proven this truth. According to Kasiri and Fathi [43], the highest percentages of charred residue were found in pistachio shells (29.9%), treated pistachio shells (22.5%), and CNCs (27.2%) [43]. The results for thermal stability in the present work generally agreed with those from FTIR, SEM, and XRD data.

3.6 Crystallinity analysis

An XRD analysis of raw fiber, treated fiber, and CNCs extracted from the *Ensete ventricosum* pseudo-stem was performed. Figure 5 and Table 4 reveal different peak patterns for all samples. This might be due to the presence of different chemical components for each sample at different treatment stages. Due to the presence of non-cellulosic constituents such as hemicellulose, extractives, and lignin in raw EVPSF, which were removed in subsequent pretreatments, semicrystalline broad amorphous humps and crystalline peaks were observed [26]. From experimental data, peaks were observed at about 15.74, 16.80, 22.65, and 34.50°, and the CI was found to be about 44.09, 62.30, and 77.25% for raw, treated EVPSF, and isolated CNCs, respectively. There are also very smaller peaks shown at 43.98, 64.32, and 77.40°. As clearly observed from the figure and the data, the crystallinity of the sample increases with stepwise chemical pretreatments. This situation witnessed the effectiveness of methods used to remove non-cellulosic parts. Amorphous components such as hemicellulose and lignin effectively dissolve through alkali treatments and the crystallinity of the sample significantly increases (Hemmati et al., 2018a,[53, 79]. The remaining amorphous region of cellulose, which is randomly oriented, is easily attacked by sulfuric acid due to the penetration of hydronium ions into amorphous regions. This, in turn, promotes the hydrolysis and breakdown of cellulose glycosidic bonds, resulting in the formation of independent crystallites [26, 61]. Figure revealed that the removal of the amorphous domain of cellulose increases the CI of CNCs and gives narrower and sharper peaks. In all sample patterns, type I cellulose existed dominantly [25]. Peaks at $2\theta = (16.38°$, 101 plane), (22.58°, 002 plane), and (34.89°, 004 plane). Type II cellulose was also observed at a peak of 22°, 002 plane. This may be associated with the re-precipitation of cellulose after sulfuric acid hydrolysis [25, 26]. The average crystallite size of CNCs was determined as 52.41 nm using the Scherrer equation (Eq. 13). The result was deviated a little bit from the result obtained from the particle size analyzer (66.8). This might have occurred due to personal error, value of constants ($k = 0.89$ to 1.39), or instrumental error. Generally, the results for CNCs reveal that the final product is homogenously distributed and has a roughly spherical shape (Table 4).

The present work's result is in good agreement with so many works [11, 25, 26, 69]. Normand et al. [66] reported

Table 4 XRD data of the raw, treated EVPSF, and isolated CNCs

Sample			Percent crystallinity index (CI)			
Raw EVPSF			44.0862			
Treated EVPSF			62.30			
Isolated CNCs			77.247			
K	**λ**	**Peak position (2θ)**		**FWHM**	**L**	
	Å	°		°	nm	
1.39	1.5418	15.84725		6.24238	1.98601	
1.39	1.5418	77.47805		0.41489	37.94333	
1.39	1.5418	64.35972		0.31724	45.73113	
1.39	1.5418	43.99403		0.21975	60.2645	
1.39	1.5418	34.52006		2.88145	4.46237	
1.39	1.5418	22.57454		1.82869	6.84712	

three different XRD peaks with different intensities as 16.1, 22.5, and 34.5° [66], also showed three peaks as 16.8, 22.8, and 34.6° (Hemmati et al., 2018a); and Sai Prasanna and Mitra [80] were another researcher who reported XRD peaks as 15.1, 21.5, and 36.6 [80], for samples at 101, 002, and 004 planes, respectively.

3.7 Morphological analysis

The shape and morphology of the raw, treated, and extracted cellulose nanocrystals of *EVPSF* are illustrated in Fig. 6. According to SEM micrographs in Fig. 6, there exist clear differences between the morphologies of raw and treated *Ensete* fiber and isolated CNCs. The raw EVPSF image (Fig. 6a) has a smoother surface, which was expected given the presence of extractives such as wax, pectin, hemicellulose, and lignin [28, 44, 66]. In contrast to raw fiber, treated *Ensete* fiber showed a rough surface with chunks of fiber bundles and an irregular shape and size. This is mainly because of degradation of non-cellulosic parts of the fiber by chemical pretreatments, which indicates the removal of the shielding coat that covers alpha cellulose [28]. These shielding coats are mainly lignin and hemicellulose [44, 66, 72]. As the image clearly illustrates, the removal of these covering structures of cellulose leaves so many pores and a rough surface that enhances the penetration of sulfuric acid into the inner parts of cellulose during acid hydrolysis [66, 78]. Thus, pretreatment methods and their treatment conditions play a significant role in determining the yield and properties of CNCs [66]. Figure 6c reveals that cellulose nanocrystals have a defined shape that resembles a rod structure and the figure also shows some clusters of CNCs [66].

4 Conclusion

Cellulose nanocrystals were successfully extracted from EVPSF's cellulose, a plentiful, inexpensive, and easily accessible material. The present study looked at how the functional group, size, surface charge, chemical composition, morphology, thermal properties, and crystallinity of EVPSF changed during mechanical and chemical pretreatment, and sulfuric acid hydrolysis, as well as how the hydrolysis condition affected the yield and properties of CNCs. The efficient and progressive removal of hemicellulose and lignin from the biomass resulted in a high amount of cellulose, which facilitates the subsequent extraction of CNCs. Chemical pretreatments and sulfuric acid hydrolysis conditions have a significant impact on CNC yield. Proper reaction conditions for both chemical pretreatment and acid hydrolysis of cellulose are thus critical considerations for obtaining good CNCs yield and properties. The

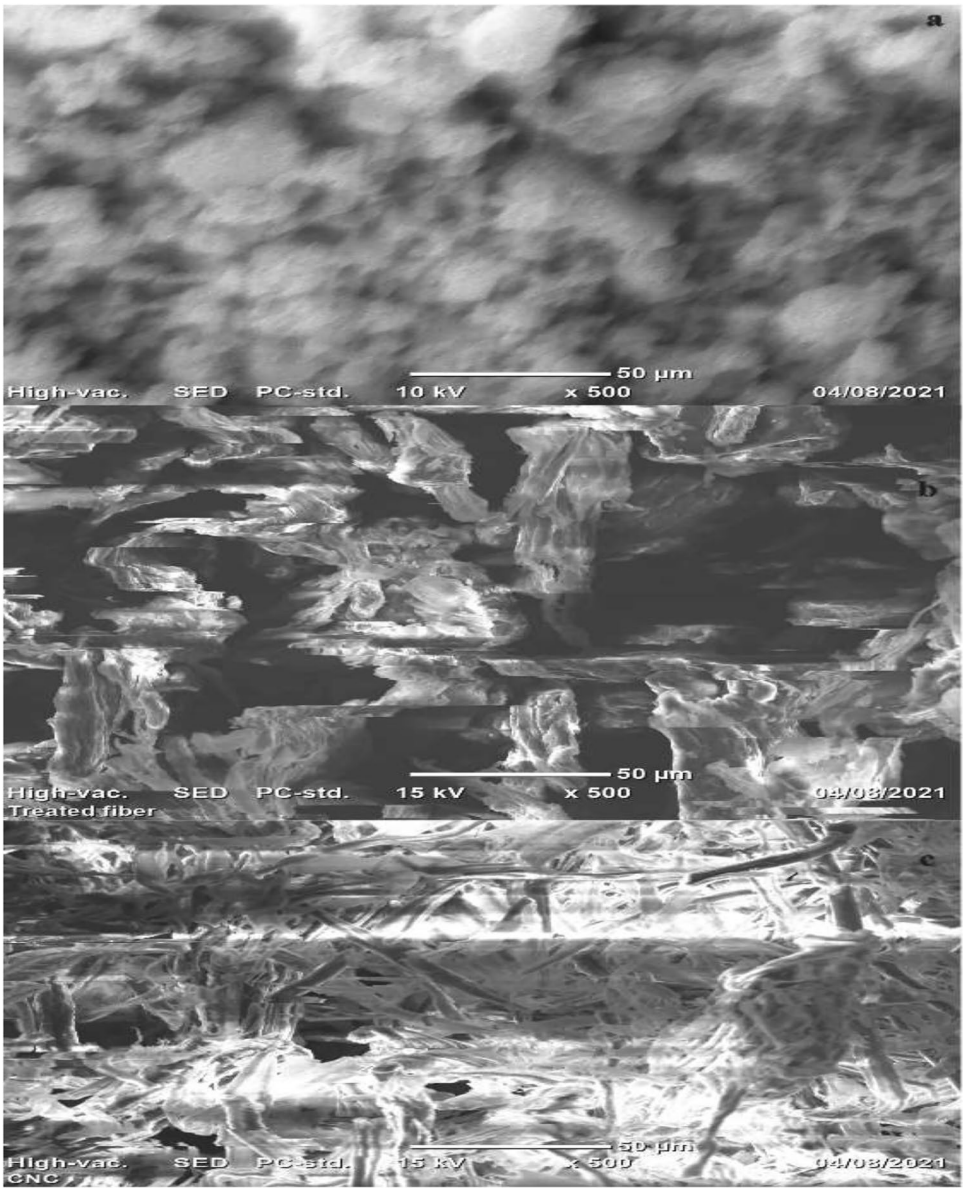

Fig. 6 SEM image of raw (**a**), treated (**b**) EVPSF, and extracted CNCs (**c**)

results for various characterizations show that EVPSF is an effective, sustainable, and renewable source for cellulose nanocrystal isolation. The optimum hydrolysis values for sulfuric acid concentration, hydrolysis temperature, and time for CNCs isolation were 51% wt., 52 °C, and 51 min, respectively. The obtained cellulose nanocrystals' good thermal stability, nano-size diameter, and high CI indicate a significant potential for use as reinforcement in polymeric composites for a variety of applications.

Acknowledgements The author is grateful for financial support from Wolkite University (WKU) and the Ethiopian Ministry of Science and Higher Education (MOSHE), as well as technical support from Addis Ababa Science and Technology University (AASTU).

Author contribution The experiment was conducted by A.M.Dube, who also gathered data, evaluated the data, drafted the manuscript, and wrote the final manuscript.

Declarations

Conflict of interest The author declares no competing interests.

References

1. A Brandt, SA Spring, A Hiebsch C Mccabe, JT Tabogie, E Diro, M Wolde-Michael, G Yntiso, G Shigeta, M & Tesfaye, S (1997) *Tree against hunger enset-based agricultural systems in Ethiopia*

American Association for the Advancement of Science http://hdl.handle.net/123456789/1284
2. Abraham E, Deepa B, Pothan LA, Jacob M, Thomas S, Cvelbar U, Anandjiwala R (2011) Extraction of nanocellulose fibrils from lignocellulosic fibres: a novel approach. Carbohyd Polym 86(4):1468–1475. https://doi.org/10.1016/j.carbpol.2011.06.034
3. Aguayo MG, Pérez AF, Reyes G, Oviedo C, Gacitúa W, Gonzalez R, & Uyarte O (2018). Isolation and characterization of cellulose nanocrystals from rejected fibers originated in the Kraft Pulping process. *Polymers*, *10*(10). https://doi.org/10.3390/polym10101145
4. Aldaeus F, & Sjöholm E (2011). *COST action FP0901 round robins of lignin samples part 1 : lignin* content (Issue December).
5. Alemdar A, Sain M (2008) Isolation and characterization of nanofibers from agricultural residues—wheat straw and soy hulls. Biores Technol 99(6):1664–1671. https://doi.org/10.1016/j.biortech.2007.04.029
6. Ali JB, Danladi A, Bukhari MM, Nyakuma BB, Mamza P, Mohamad ZB, Musa AB, Inuwa IM (2020) Extraction and characterization of cellulose nanofibres and cellulose nanocrystals from Sammaz-14 maize cobs. J Nat Fibers 00(00):1–16. https://doi.org/10.1080/15440478.2020.1856279
7. Araki J, Wada M, Kuga S, Okano T (1998) Flow properties of microcrystalline cellulose suspension prepared by acid treatment of native cellulose. Colloids Surf A Physicochem Eng Asp 142(1):75–82. https://doi.org/10.1016/S0927-7757(98)00404-X
8. Ashori A, Hamzeh Y, & Amani F (2011). *Lemon balm (Melissa officinalis) stalk: chemical composition and fiber* morphology. 297–300. https://doi.org/10.1007/s10924-010-0279-8
9. Asrofi M, Abral H, Kasim A, Pratoto A, Mahardika M, Park JW, Kim HJ (2018) Isolation of nanocellulose from water hyacinth fiber (WHF) produced via digester-sonication and its characterization. Fibers Polym 19(8):1618–1625. https://doi.org/10.1007/s12221-018-7953-1
10. Aziz T, Fan H, Zhang X, Haq F, Ullah A, Ullah R, Khan FU, Iqbal M (2020) Advance study of cellulose nanocrystals properties and applications. J Polym Environ 28(4):1117–1128. https://doi.org/10.1007/s10924-020-01674-2
11. Bano S, Negi YS (2017) Studies on cellulose nanocrystals isolated from groundnut shells. Carbohyd Polym 157:1041–1049. https://doi.org/10.1016/j.carbpol.2016.10.069
12. Beck-Candanedo S, Roman M, Gray DG (2005) Effect of reaction conditions on the properties and behavior of wood cellulose nanocrystal suspensions. Biomacromol 6(2):1048–1054. https://doi.org/10.1021/bm049300p
13. Berhanu H, Kiflie Z, Miranda I, Lourenço A, Ferreira J, Feleke S, Yimam A, & Pereira H (2018a). Characterization of crop residues from false banana/ensete ventricosum/in Ethiopia in view of a full-resource valorization. *PLoS ONE*, *13*(7). https://doi.org/10.1371/journal.pone.0199422
14. Berhanu H, Kiflie Z, Miranda I, Lourenço A, Ferreira J, Feleke S, Yimam A, & Pereira H (2018b). Characterization of crop residues from false banana/ensete ventricosum/in Ethiopia in view of a full-resource valorization. *PLoS ONE*, *13*(7). https://doi.org/10.1371/journal.pone.0199422
15. Birmeta G, Bakeeva A, Passoth V (2019) Yeasts and bacteria associated with kocho, an Ethiopian fermented food produced from enset (Ensete ventricosum). Antonie Van Leeuwenhoek 112(4):651–659. https://doi.org/10.1007/s10482-018-1192-8
16. Borrell JS, Biswas MK, Goodwin M, Blomme G, Schwarzacher T, Heslop-Harrison JS, Wendawek AM, Berhanu A, Kallow S, Janssens S, Molla EL, Davis AP, Woldeyes F, Willis K, Demissew S, Wilkin P (2019) Enset in Ethiopia: a poorly characterized but resilient starch staple. Ann Bot 123(5):747–766. https://doi.org/10.1093/aob/mcy214
17. Brinchi L, Cotana F, Fortunati E, Kenny JM (2013) Production of nanocrystalline cellulose from lignocellulosic biomass: technology and applications. Carbohyd Polym 94(1):154–169. https://doi.org/10.1016/j.carbpol.2013.01.033
18. Buchanan M (2012). Solvent extractives of wood and pulp (proposed revision of TAPPI T 204 cm-97). In *Nanofibers* — production*, properties and functional applications*.
19 Chen Y, Wu Q, Huang B, Huang M, Ai X (2015) Isolation and characteristics of cellulose and nanocellulose from lotus leaf stalk agro-wastes. BioResources 10(1):684–696. https://doi.org/10.15376/biores.10.1.684-696
20. Chirayil CJ, Joy J, Mathew L, Mozetic M, Koetz J, Thomas S (2014) Isolation and characterization of cellulose nanofibrils from Helicteres isora plant. Ind Crops Prod 59:27–34. https://doi.org/10.1016/j.indcrop.2014.04.020
21. Collazo-Bigliardi S, Ortega-Toro R, & Chiralt Boix A. (2018). Isolation and characterisation of microcrystalline cellulose and cellulose nanocrystals from coffee husk and comparative study with rice husk. *Carbohydrate Polymers*, *191* (October 2017), 205–215. https://doi.org/10.1016/j.carbpol.2018.03.022
22. De Sá RM, De Miranda CS, José NM (2015) Preparation and characterization of nanowhiskers cellulose from fiber arrowroot (Maranta arundinacea). Mater Res 18(Suppl 2):225–229. https://doi.org/10.1590/1516-1439.366214
23. Dong XM, Revol JF, Gray DG (1998) Effect of microcrystallite preparation conditions on the formation of colloid crystals of cellulose. Cellulose 5(1):19–32. https://doi.org/10.1023/A:1009260511939
24. Elanthikkal S, Gopalakrishnapanicker U, Varghese S, Guthrie JT (2010) Cellulose microfibres produced from banana plant wastes: isolation and characterization. Carbohyd Polym 80(3):852–859. https://doi.org/10.1016/j.carbpol.2009.12.043
25. Espino E, Cakir M, Domenek S, Román-Gutiérrez AD, Belgacem N, Bras J (2014) Isolation and characterization of cellulose nanocrystals from industrial by-products of Agave tequilana and barley. Ind Crops Prod 62:552–559. https://doi.org/10.1016/j.indcrop.2014.09.017
26. Flauzino Neto WP, Silvério HA, Dantas NO, Pasquini D (2013) Extraction and characterization of cellulose nanocrystals from agro-industrial residue — soy hulls. Ind Crops Prod 42(1):480–488. https://doi.org/10.1016/j.indcrop.2012.06.041
27. Gabriel T, Belete A, Syrowatka F, Neubert RHH, Gebre-Mariam T (2020) Extraction and characterization of celluloses from various plant byproducts. Int J Biol Macromol 158:1248–1258. https://doi.org/10.1016/j.ijbiomac.2020.04.264
28. Galiwango E, Abdel NS, Al-marzouqi AH, Abu-omar MM, Khaleel AA (2019) Heliyon isolation and characterization of cellulose and α-cellulose from date palm biomass waste. Heliyon 5(July):e02937. https://doi.org/10.1016/j.heliyon.2019.e02937
29. Garcia de Rodriguez NL, Thielemans W, Dufresne A (2006) Sisal cellulose whiskers reinforced polyvinyl acetate nanocomposites. Cellulose 13(3):261–270. https://doi.org/10.1007/s10570-005-9039-7
30. George J, Ramana KV, Bawa AS, Siddaramaiah. (2011) Bacterial cellulose nanocrystals exhibiting high thermal stability and their polymer nanocomposites. Int J Biol Macromol 48(1):50–57. https://doi.org/10.1016/j.ijbiomac.2010.09.013
31. Gong J, Li J, Xu J, Xiang Z, Mo L (2017) Research on cellulose nanocrystals produced from cellulose sources with various polymorphs. RSC Adv 7(53):33486–33493. https://doi.org/10.1039/c7ra06222b
32. Habibi Y, Lucia LA, Rojas OJ (2010) Cellulose nanocrystals: chemistry, self-assembly, and applications. Chem Rev 110(6):3479–3500. https://doi.org/10.1021/cr900339w

33. Hemmati F, Jafari SM, Kashaninejad M, Barani Motlagh M (2018) Synthesis and characterization of cellulose nanocrystals derived from walnut shell agricultural residues. Int J Biol Macromol 120:1216–1224. https://doi.org/10.1016/j.ijbiomac.2018.09.012
34. Hendriks ATWM, Zeeman G (2009) Pretreatments to enhance the digestibility of lignocellulosic biomass. Biores Technol 100(1):10–18. https://doi.org/10.1016/j.biortech.2008.05.027
35. Hernandez, C. C., & Rosa, D. S. (2016). Extraction of cellulose nanowhiskers: natural fibers source, methodology and application. Polymer Science: Research Advances, Practical Applications and Educational Aspects, July, 232–242. https://www.researchgate.net/publication/305318996
36. Ilyas RA, Sapuan SM., & Ishak MR. (2018a). Isolation and characterization of nanocrystalline cellulose from sugar palm fibres (Arenga pinnata). *Carbohydrate Polymers*, *181*(June 2017), 1038–1051.https://doi.org/10.1016/j.carbpol.2017.11.045
37. Ilyas RA, Sapuan SM, Ishak MR (2018) Isolation and characterization of nanocrystalline cellulose from sugar palm fibres (Arenga pinnata). Carbohyd Polym 181:1038–1051. https://doi.org/10.1016/j.carbpol.2017.11.045
38. Jiang F, Hsieh YL (2013) Chemically and mechanically isolated nanocellulose and their self-assembled structures. Carbohyd Polym 95(1):32–40. https://doi.org/10.1016/j.carbpol.2013.02.022
39. Johar N, Ahmad I, Dufresne A (2012) Extraction, preparation and characterization of cellulose fibres and nanocrystals from rice husk. Ind Crops Prod 37(1):93–99. https://doi.org/10.1016/j.indcrop.2011.12.016
40. KJN Balaji AN & Ramanujam NR (2020) Isolation and characterization of cellulose nanocrystals from Saharan aloe vera cactus fibers. Int J Polym Anal Charact 25(2):51–64. https://doi.org/10.1080/1023666X.2018.1478366
41. Kallel F, Bettaieb F, Khiari R, García A, Bras J, Chaabouni SE (2016) Isolation and structural characterization of cellulose nanocrystals extracted from garlic straw residues. Ind Crops Prod 87:287–296. https://doi.org/10.1016/j.indcrop.2016.04.060
42. Kargarzadeh H, Ahmad I, Abdullah I, Dufresne A, Zainudin SY, Sheltami RM (2012) Effects of hydrolysis conditions on the morphology, crystallinity, and thermal stability of cellulose nanocrystals extracted from kenaf bast fibers. Cellulose 19(3):855–866. https://doi.org/10.1007/s10570-012-9684-6
43. Kasiri N, Fathi M (2018) Production of cellulose nanocrystals from pistachio shells and their application for stabilizing Pickering emulsions. Int J Biol Macromol 106:1023–1031. https://doi.org/10.1016/j.ijbiomac.2017.08.112
44. Kathirselvam M, Kumaravel A, Arthanarieswaran VP, Saravanakumar SS (2019) International journal of biological macromolecules isolation and characterization of cellulose fibers from Thespesia populnea barks: a study on physicochemical and structural properties. Int J Biol Macromol 129:396–406. https://doi.org/10.1016/j.ijbiomac.2019.02.044
45. Kia L, Jawaid M, Arif H, Karim Z (2018) International journal of biological macromolecules isolation and characterization of nanocrystalline cellulose from roselle-derived microcrystalline cellulose 114:54–63. https://doi.org/10.1016/j.ijbiomac.2018.03.065
46. Klemm D, Cranston ED, Fischer D, Gama M, Kedzior SA, Kralisch D, Kramer F, Kondo T, Lindström T, Nietzsche S, Petzold-Welcke K, Rauchfuß F (2018) Nanocellulose as a natural source for groundbreaking applications in materials science: today's state. Mater Today 21(7):720–748. https://doi.org/10.1016/j.mattod.2018.02.001
47. Klemm D, Kramer F, Moritz S, Lindström T, Ankerfors M, Gray D, Dorris A (2011) Nanocelluloses: a new family of nature-based materials. Angewandte Chemie - International Edition 50(24):5438–5466. https://doi.org/10.1002/anie.201001273
48. Larissa LA, Fonsêca AF, Pereira FV, Druzian JI (2015) Extraction and characterization of cellulose nanocrystals from corn stover. Cellul Chem Technol 49(2):127–133
49. Lu P, Hsieh YL (2012) Preparation and characterization of cellulose nanocrystals from rice straw. Carbohyd Polym 87(1):564–573. https://doi.org/10.1016/j.carbpol.2011.08.022
50. Lu P, Hsieh Y (2010) Preparation and properties of cellulose nanocrystals: rods, spheres, and network. Carbohyd Polym 82(2):329–336. https://doi.org/10.1016/j.carbpol.2010.04.073
51. Mandal A, Chakrabarty D (2011) Isolation of nanocellulose from waste sugarcane bagasse (SCB) and its characterization. Carbohyd Polym 86(3):1291–1299. https://doi.org/10.1016/j.carbpol.2011.06.030
52. Marett J, Aning A, Foster EJ (2017) Industrial crops & products the isolation of cellulose nanocrystals from pistachio shells via acid hydrolysis Abnet Mengesha. Ind Crops Prod 109(June):869–874. https://doi.org/10.1016/j.indcrop.2017.09.039
53. Marett J, Aning A, Foster EJ (2017) The isolation of cellulose nanocrystals from pistachio shells via acid hydrolysis. Ind Crops Prod 109(October):869–874. https://doi.org/10.1016/j.indcrop.2017.09.039
54. Mariano M, Cercená R, Soldi V (2016) Thermal characterization of cellulose nanocrystals isolated from sisal fibers using acid hydrolysis. Ind Crops Prod 94:454–462. https://doi.org/10.1016/j.indcrop.2016.09.011
55. Martins DF, De Souza AB, Henrique MA, Silvério HA, Pires W, Neto F, Pasquini D (2015) The influence of the cellulose hydrolysis process on the structure of cellulose nanocrystals extracted from capim mombaca (Panicum maximum). Ind Crops Prod 65:496–505. https://doi.org/10.1016/j.indcrop.2014.10.035
56. Mendes CADC, Ferreira NMS, Furtado CRG, De Sousa AMF (2015) Isolation and characterization of nanocrystalline cellulose from corn husk. Mater Lett 148:26–29. https://doi.org/10.1016/j.matlet.2015.02.047
57. Merci A, Urbano A, Victória M, Grossmann E, Tischer CA (2015) Properties of microcrystalline cellulose extracted from soybean hulls by reactive extrusion. FRIN 73:38–43. https://doi.org/10.1016/j.foodres.2015.03.020
58. Morais JPS, Rosa MDF, De Souza Filho MDSM, Nascimento LD, Do Nascimento DM, Cassales AR (2013) Extraction and characterization of nanocellulose structures from raw cotton linter. Carbohyd Polym 91(1):229–235. https://doi.org/10.1016/j.carbpol.2012.08.010
59. Mueller S, Weder C, Foster EJ (2014) Isolation of cellulose nanocrystals from pseudostems of banana plants. RSC Adv 4(2):907–915. https://doi.org/10.1039/c3ra46390g
60. Naduparambath S, TV J, Shaniba V, MP S Balan, AK, & Purushothaman E (2018a). Isolation and characterisation of cellulose nanocrystals from sago seed shells. *Carbohydrate Polymers*, *180* April 2017 13–20. https://doi.org/10.1016/j.carbpol.2017.09.088
61. Naduparambath S, TV J, Shaniba V, MP S, Balan A K, & Purushothaman E (2018b). Isolation and characterisation of cellulose nanocrystals from sago seed shells. *Carbohydrate Polymers*, *180*(September 2017), 13–20. https://doi.org/10.1016/j.carbpol.2017.09.088
62. Nagarajan KJ, Balaji AN, Ramanujam NR, & Thanga Kasi Rajan S (2019). Preparation and characterization of alkali treated cocos nucifera var aurantiaca peduncle fibers reinforced epoxy composites. *Materials Research Express*, *6*(12). https://doi.org/10.1088/2053-1591/ab54ff
63. Nagarajan KJ, Balaji AN, Thanga Kasi Rajan S, & Sathick Basha K (2019). Effect of sulfuric acid reaction time on the properties and behavior of cellulose nanocrystals from Cocos nucifera

var-Aurantiaca peduncle's cellulose microfibers. *Materials Research Express*, *6*(12). https://doi.org/10.1088/2053-1591/ab5a9d
64. Nagarajan KJ, Ramanujam NR, Sanjay MR, Siengchin S, Surya Rajan B, Sathick Basha K, Madhu P, & Raghav GR (2021). A comprehensive review on cellulose nanocrystals and cellulose nanofibers: pretreatment, preparation, and characterization. In *Polymer Composites* (Vol. 42, Issue 4). https://doi.org/10.1002/pc.25929
65. Nanda S, Mohanty P, Pant KK, Naik S, Kozinski JA, Dalai AK (2013) Characterization of North American lignocellulosic biomass and biochars in terms of their candidacy for alternate renewable fuels. Bioenergy Res 6(2):663–677. https://doi.org/10.1007/s12155-012-9281-4
66. Normand ML, Moriana R, Ek M (2014) Isolation and characterization of cellulose nanocrystals from spruce bark in a biorefinery perspective. Carbohyd Polym 111:979–987. https://doi.org/10.1016/j.carbpol.2014.04.092
67. Nurfeta A, Eik LO, Tolera A, & Sundstøl F (2008). Chemical composition and in sacco dry matter degradability of different morphological fractions of 10 enset (Ensete ventricosum) varieties. 146, 55–73. https://doi.org/10.1016/j.anifeedsci.2007.12.003
68. Nurfeta A, Tolera A, Eik LO, Sundstøl F (2008) Yield and mineral content of ten enset (Ensete ventricosum) varieties. Trop Anim Health Prod 40(4):299–309. https://doi.org/10.1007/s11250-007-9095-0
69. Oun AA, Rhim J (2016) Isolation of cellulose nanocrystals from grain straws and their use for the preparation of carboxymethyl cellulose-based nanocomposite films. Carbohyd Polym 150:187–200. https://doi.org/10.1016/j.carbpol.2016.05.020
70. Pereira B, & Arantes V (2018). Nanocelluloses from sugarcane biomass. In *Advances in sugarcane biorefinery: technologies, commercialization, policy issues and paradigm shift for bioethanol and by-products* (pp. 179–196). https://doi.org/10.1016/B978-0-12-804534-3.00009-4
71. Persat A, Chambers RD, Santiago JG (2009) Basic principles of electrolyte chemistry for microfluidic electrokinetics Part I acid-base equilibria and pH buffers. Lab on a Chip 9(17):2437–2453. https://doi.org/10.1039/b906465f
72. Pires W, Neto F, Alves H, Oliveira N, Pasquini D (2013) Extraction and characterization of cellulose nanocrystals from agro-industrial residue — soy hulls. Ind Crops Prod 42:480–488. https://doi.org/10.1016/j.indcrop.2012.06.041
73. Prado KS, Spinacé MAS (2019) Isolation and characterization of cellulose nanocrystals from pineapple crown waste and their potential uses. Int J Biol Macromol 122:410–416. https://doi.org/10.1016/j.ijbiomac.2018.10.187
74. Prasanna NS, Mitra J (2020) Isolation and characterization of cellulose nanocrystals from Cucumis sativus peels. Carbohyd Polym 247(July):116706. https://doi.org/10.1016/j.carbpol.2020.116706
75. Qiao C, Chen G, Zhang J, Yao J (2016) Structure and rheological properties of cellulose nanocrystals suspension. Food Hydrocolloids 55:19–25. https://doi.org/10.1016/j.foodhyd.2015.11.005
76. Rahman NHA, Chieng BW, Ibrahim NA, Rahman NA (2017) Extraction and characterization of cellulose nanocrystals from tea leaf waste fibers. Polymers 9(11):1–11. https://doi.org/10.3390/polym9110588
77. Ray D, Sarkar BK, Rana AK, Bose NR (2001) Effect of alkali treated jute fibres on composite properties. Bull Mater Sci 24(2):129–135. https://doi.org/10.1007/BF02710089
78. Reddy JP, Rhim J (2014) Isolation and characterization of cellulose nanocrystals from garlic skin. Mater Lett 129:20–23. https://doi.org/10.1016/j.matlet.2014.05.019
79. S, J. C. C., George, N., & Narayanankutty, S. K. (2016) Isolation and characterization of cellulose nanofibrils from arecanut husk fibre. Carbohyd Polym 142:158–166. https://doi.org/10.1016/j.carbpol.2016.01.015
80. Sai Prasanna N, Mitra J (2020) Isolation and characterization of cellulose nanocrystals from Cucumis sativus peels. Carbohyd Polym 247(March):116706. https://doi.org/10.1016/j.carbpol.2020.116706
81. dos Santos RM, Flauzino Neto WP, Silvério HA, Martins DF, Dantas NO, Pasquini D (2013) Cellulose nanocrystals from pineapple leaf, a new approach for the reuse of this agro-waste. Ind Crops Prod 50:707–714. https://doi.org/10.1016/j.indcrop.2013.08.049
82. Segal L, Creely JJ, Martin AE, Conrad CM (1959) An empirical method for estimating the degree of crystallinity of native cellulose using the X-ray diffractometer. Text Res J 29(10):786–794. https://doi.org/10.1177/004051755902901003
83. Sheltami RM, Abdullah I, Ahmad I, Dufresne A, Kargarzadeh H (2012) Extraction of cellulose nanocrystals from mengkuang leaves (Pandanus tectorius). Carbohyd Polym 88(2):772–779. https://doi.org/10.1016/j.carbpol.2012.01.062
84. Silvério HA, Flauzino Neto WP, Dantas NO, Pasquini D (2013) Extraction and characterization of cellulose nanocrystals from corncob for application as reinforcing agent in nanocomposites. Ind Crops Prod 44:427–436. https://doi.org/10.1016/j.indcrop.2012.10.014
85. Smyth M, García A, Rader C, Foster EJ, Bras J (2017) Extraction and process analysis of high aspect ratio cellulose nanocrystals from corn (Zea mays) agricultural residue. Ind Crops Prod 108(June):257–266. https://doi.org/10.1016/j.indcrop.2017.06.006
86. Song K, Zhu X, Zhu W, & Li X (2019). Preparation and characterization of cellulose nanocrystal extracted from Calotropis procera biomass. *Bioresources and Bioprocessing*, *6*(1). https://doi.org/10.1186/s40643-019-0279-z
87. Sun Y, Cheng J (2002) Hydrolysis of lignocellulosic materials for ethanol production: a review. Biores Technol 83(1):1–11. https://doi.org/10.1016/S0960-8524(01)00212-7
88. Tappi. (2007). Solvent extractives of wood and pulp (Proposed revision of T 204 cm-97). *Tappi*.
89. TAPPI. (2017). TAPPI T211 om-02: ash in wood, pulp paper and paperboard: combustion at 525°C. In *TAPPI Test Methods 2005*.
90. TAPPI International Nanotecnology Division, & Division, I. N. (2011). Roadmap for the development of international standards for nanocellulose. *Tappi*, 33 https://www.tappinano.org/whats-up/standards-summary
91. Tappi T 204 cm-97. (1997). Solvent extractives of wood and pulp (Proposed revision of T 204 cm-97). *Tappi*.
92. Technical Association of Pulp and Paper Industry. (2006). Acid-insoluble lignin in wood and pulp (T222 Om-02). *TAPPI Standards*.
93. de Teixeira E, M., Bondancia, T. J., Teodoro, K. B. R., Corrêa, A. C., Marconcini, J. M., & Mattoso, L. H. C. (2011) Sugarcane bagasse whiskers: extraction and characterizations. Ind Crops Prod 33(1):63–66. https://doi.org/10.1016/j.indcrop.2010.08.009
94. Teli, M. D., & Terega, J. M. (2017a). Chemical, physical and thermal characterization of Ensete ventricosum plant fibre. *International Research Journal of Engineering and Technology*, *04*(12) www.irjet.net
95. Teli MD, & Terega JM (2017b). Chemical, physical and thermal characterization of Ensete ventricosum plant fibre. *International Research Journal of Engineering and Technology*, *04*(12), 67–75. www.irjet.net
96. Thambiraj S, Ravi Shankaran D (2017) Preparation and physicochemical characterization of cellulose nanocrystals from industrial waste cotton. Appl Surf Sci 412:405–416. https://doi.org/10.1016/j.apsusc.2017.03.272
97. Thygesen A, Oddershede J, Lilholt H, Thomsen AB, Ståhl K (2005) On the determination of crystallinity and cellulose content

in plant fibres. Cellulose 12(6):563–576. https://doi.org/10.1007/s10570-005-9001-8
98. Vijay R, Lenin Singaravelu D, Vinod A, Sanjay MR, Siengchin S, Jawaid M, Khan A, Parameswaranpillai J (2019) Characterization of raw and alkali treated new natural cellulosic fibers from Tridax procumbens. Int J Biol Macromol 125:99–108. https://doi.org/10.1016/j.ijbiomac.2018.12.056
99. Wang X, Yao C, Wang F, Li Z (2017) Cellulose-based nanomaterials for energy applications. Small 13(42):1–19. https://doi.org/10.1002/smll.201702240
100. Wu Y, Wu J, Yang F, Tang C, Huang Q (2019) Effect of H2O2 bleaching treatment on the properties of finished transparent wood. Polymers 11(5):1–13. https://doi.org/10.3390/polym11050776
101. Yemata G. (2020). Ensete ventricosum: a multipurpose crop against hunger in Ethiopia. In *Scientific World Journal* (Vol. 2020). Hindawi Limited. https://doi.org/10.1155/2020/6431849
102. Zeronian SH, Inglesby MK (1995) Bleaching of cellulose by hydrogen peroxide. Cellulose 2(4):265–272. https://doi.org/10.1007/BF00811817
103. Zhang H, Chen Y, Wang S, Ma L, Yu Y, Dai H, Zhang Y (2020) Extraction and comparison of cellulose nanocrystals from lemon (Citrus limon) seeds using sulfuric acid hydrolysis and oxidation methods. Carbohyd Polym 238(2):116180. https://doi.org/10.1016/j.carbpol.2020.116180
104. Zhang Q, Zhang P, Pei ZJ, Wang D (2013) Relationships between cellulosic biomass particle size and enzymatic hydrolysis sugar yield: analysis of inconsistent reports in the literature. Renewable Energy 60:127–136. https://doi.org/10.1016/j.renene.2013.04.012